Isogeometric homogenization of viscoelastic polymer composites via correspondence principle

Qiang Chen[a,b], Xiaoxiao Du[c]*, Wei Wang[c], George Chatzigeorgiou[b], Fodil Meraghni[b], Gang Zhao[d]

[a]School of Mechanical Engineering, Xi'an Jiaotong University, Xi'an, Shaanxi, 710049, PR China

[b]Arts et Métiers Institute of Technology, CNRS, Université de Lorraine, LEM3-UMR7239, F-57000 Metz, France

[c]School of Mechanical Engineering and Automation, Beihang University, Beijing 100191, PR China

[d]Tsinghua University, Beijing, 100084, PR China

Corresponding author: duxiaoxiao@buaa.edu.cn

Abstract

We present an isogeometric homogenization theory (IGH) for efficiently identifying homogenized and local creep and relaxation response of linearly viscoelastic polymer composites with different microstructural parameters. The principal idea is to construct exact geometric representations of both two- and three-dimensional unit cell microstructures for periodic materials by utilizing multiple conforming NURBS patches that are also employed for the displacement field interpolation function at the local scale. The IGH-based unit cell formulation is then converted to the viscoelastic solution with the Laplace-Carson space parameters via the correspondence principle. Subsequently, we leverage the Zakian formula to reverse the transformed IGH solution and obtain the homogenized creep and relaxation response of the composite in the original time space. The modelling and predictive capabilities of the IGH theory have been extensively validated vis-à-vis the elasticity-based and conventional finite-element homogenization techniques, and the advantages of the proposed technique over the reference techniques were demonstrated.

Keywords: Polymer composites; Isogeometric analysis; Homogenization theory; Viscoelasticity; Micromechanics

1. Introduction

The growing utilization of polymeric composites in a broad range of applications, such as aerospace, wind energy, marine, and automotive industries, requires the development of computational tools to quantify their long-term behavior. The polymer composites are viscoelastic and heterogeneous solids, exhibiting important creep and relaxation phenomena that are characterized by the instant elastic and viscous response that changes over time. The latter significantly affects the durability and sustainability of the polymer composites [1-3]. Therefore, the investigation of the relaxation and creep behavior of the polymer composite materials at the global and constituent phase levels is crucial for efficiently designing durable and sustainable composite components that cater to the particular requirements of various applications. However,

conducting experimental assessments of the long-term behavior of polymer composites is an arduous and expensive process. Hence it is only feasible for a restricted range of material combinations and volume fractions.

The use of homogenization approaches is an appealing alternative to the experimental characterization of the effective creep and relaxation response of polymer composites containing varying combinations of reinforcement and matrix properties and volume fractions [4, 5]. Although the simple micromechanics and homogenization theories, namely, the cylindrical cylinder/sphere assemblage (CCA) [6], the generalized self-consistent method [7], and the Mori-Tanaka method (MT) [8], are effective in predicting the homogenized elastic stiffness tensor of fiber- or particle-reinforced composite materials across a broad range of volume fractions, they fail to provide precise local stress fields and thus the homogenized inelastic response [9]. This is because the classical micromechanics models do not account for the interaction with the adjacent inclusions. The need for accurate local stress field predictions motivates the continuous development of numerical or semi-analytical models for periodic composites that require more sophisticated numerical and analytical treatments [10]. The elasticity theory-based homogenization approach that considers periodic boundary condition implementation appears to be the method of choice for local stress recovery because the stress equilibrium equations are satisfied exactly in a pointwise manner. Nevertheless, the elasticity-based periodic homogenization technique is scarce in the literature because of the inherent challenge of satisfying both displacement and traction periodicity conditions along the edges of the unit cell simultaneously. The locally-exact homogenization theory (LEHT) developed by Drago and Pindera [11] is an exception thanks to a new balanced variational technique for the implementation of periodic boundary conditions. Additional studies on the modelling of the relaxation and creep behavior of polymer composites were discovered that utilized numerical homogenization methodologies [12-16]. However, the conventional numerical techniques necessitate substantial mesh discretizations in order to precisely represent the reinforcement shape and arrangement or to satisfy the interfacial traction and displacement continuity conditions. These challenges are both essential and demanding to depict the local field variable distributions when there is a significant constituent modulus contrast. Hence, these methods are not inherently suited for analyzing heterogeneous materials.

The isogeometric analysis method (IGA), proposed by Hughes and his coworkers [17, 18], aims to unify the representation of geometric models and mesh models by directly employing the spline functions as the shape functions. The errors produced by geometric approximations inherent in conventional finite-element and finite-volume techniques could be greatly reduced because the same model is used for both modeling and analysis. Additionally, the high orders and high continuities of spline basis functions such as NURBS [19], T-spine [20], PHT-spine [21], could provide more accurate and robust results in numerical simulation even under the situation of mesh distortion [22]. The aforementioned elegant features have attracted broader attention in computational mechanics communities and make IGA a very interesting alternative for numerical simulations.

In recent years, there has been limited research on the incorporation of IGA into computational homogenization. Matsubara et al. [23] were perhaps the first to investigate the handling of heterogeneous materials and periodic boundary conditions using the IGA framework. In their work, numerical material testing (NMT) and numerical plate testing (NPT) were

successfully conducted by employing a master-slave scheme in imposing multiple-point constraints under the situation of infinitesimal deformation. Alberdi et al. [24] combined finite deformation computational homogenization and isogeometric analysis to solve representative volume element (RVE) based multiscale problems. An IGA^2 method [25] is implemented for the two-scale modelling of higher-order continua across length scales. The high-order basis functions in IGA are believed to be valuable to approximate independent fields in both micro and macro scales. Additionally, RVE-based computational homogenization in conjunction with isogeometric analysis has been successfully applied for structural simulation [26] and optimization [27].

The scope of the current manuscript is to present a zeroth-order isogeometric homogenization (IGH) theory for identifying the viscoelastic response of polymer composites with different microstructural parameters via the correspondence principle. Both two- and three-dimensional unit cells for periodic materials are constructed by utilizing multiple conforming NURBS (nonuniform rational B-splines) patches. Rather than solving the integral form of the stress-strain relation in the time domain incrementally, we leveraged the elastic-viscoelastic correspondence to convert the isogeometric unit cell formulation to the viscoelastic solution in the Laplace-Carson domain. The efficacy of implementing the correspondence principle in the IGH theory is contingent upon the efficient and accurate inversion of the Laplace-transformed unit cell solution back into the time domain. In this work, the inversion formula developed by Zakian [28] was utilized for this purpose. This is verified by an extensive comparison of the IGH predictions with those generated by the LEHT theory in the literature and the conventional finite-element techniques.

2. Theoretical framework

2.1 Elastic-viscoelastic correspondence principle for composite materials

The root idea of the elastic-viscoelastic correspondence principle for linearly viscoelastic heterogeneous media [29] is to transform the solution for the unit cell problem of periodic microstructural materials to the viscoelastic solution in the Laplace domain. To obtain the transformed solution, we substitute the displacement, strain, and stress vectors in the elastic solution with their respective Laplace transforms, $u_i \to \hat{u}_i(s)$, $\varepsilon_{ij} \to \hat{\varepsilon}_{ij}(s)$, $\sigma_{ij} \to \hat{\sigma}_{ij}(s)$, while the elastic stiffness tensor is replaced by their Carson transforms: $C_{ijkl} \to s\hat{C}_{ijkl}(s)$ with

$$\hat{C}_{ijkl}(s) = \int_0^s C_{ijkl}(t) e^{-st} \mathrm{d}t \tag{2}$$

In the above equation, s represents the Laplace variable. In the Laplace-Carson domain, the unit cell problem is formulated using the isogeometric homogenization developed in the following subsections.

2.2 NURBS basis function

NURBS has occupied the dominant position in CAD files due to its excellent properties in geometric modeling and a series of equipped algorithms. More importantly, it unifies the

mathematical expression of free-form and analytic geometries and evolves to be the unique standard for representing free-form shapes in international standards like IGES and STEP.

Given a non-decreasing knot vector $\Xi = \{\xi_1, \xi_2, \xi_3, \cdots, \xi_{n+p+1}\}$, where ξ_i is called the knot, n is the number of control points and p is the degree, a sequence of B-spline basis functions is defined recursively as [19]:

$$N_{i,0}(\xi) = \begin{cases} 1, & \xi_i \le \xi < \xi_{i+1}, \\ 0, & otherwise, \end{cases} \tag{3}$$

for $p = 0$, and

$$N_{i,p}(\xi) = \frac{\xi - \xi_i}{\xi_{i+p} - \xi_i} N_{i,p-1}(\xi) + \frac{\xi_{i+p+1} - \xi}{\xi_{i+p+1} - \xi_{i+1}} N_{i+1,p-1}(\xi) \tag{4}$$

for $p > 0$. From the above definitions, we note that the B-spline functions are piece-wise polynomial functions. For the i-th basis function, its valid parametric domain is $[\xi_i, \xi_{i+p+1}]$ and there are $p+1$ non-zero basis functions across the non-zero knot interval $[\xi_i, \xi_{i+1}]$.

Let Ξ_1 and Ξ_2 be the knot vectors in ξ and η directions with degrees p and q, respectively, a NURBS surface could be defined as

$$\boldsymbol{y}(\xi,\eta) = \sum_{A=1}^{nm} \boldsymbol{P}_A R_A(\xi,\eta), \quad R_A(\xi,\eta) = \frac{w_A N_A(\xi,\eta)}{\sum_{B=1}^{nm} w_B N_B(\xi,\eta)} \tag{5}$$

where $\boldsymbol{P}_i$ is the coordinate vector, R_i is the NURBS basis function and w_i is the weight related to the i-th control point. Parameters n and m indicate the number of control points in two directions. The function $N_A(\xi,\eta)$ is the bivariate B-spline basis functions, expressed as $N_{i,p}(\xi) N_{j,q}(\eta)$. The subscript is computed by $A = n(j-1) + i$. It should be noted that the continuities of a NURBS curve are C^{p-k} at inner knots, where k is the multiplicity of the corresponding knots.

Similarly, a trivariate NURBS solid with parameters (ξ, η, ζ) could be written as

$$\boldsymbol{y}(\xi,\eta,\zeta) = \sum_{A=1}^{nml} \boldsymbol{P}_A R_A(\xi,\eta,\zeta), \quad R_A(\xi,\eta,\zeta) = \frac{w_A N_A(\xi,\eta,\zeta)}{\sum_{B=1}^{nml} w_B N_B(\xi,\eta,\zeta)} \tag{6}$$

where the trivariate B-spline basis function $N_A(\xi,\eta,\zeta)$ is defined as $N_A(\xi,\eta,\zeta) = N_{i,p}(\xi) N_{j,q}(\eta) N_{k,r}(\zeta)$ and the subscript is given by $A = nm(k-1) + n(j-1) + i$.

2.3 Isogeometric homogenization in the Laplace-Carson domain

We center on a fundamental repeating build block or unit cell, which can be replicated in two- or three-dimensional space, depending on the microstructures under investigation. These replicated units form the complete periodic microstructural materials. The unit cell is further discretized into NURBS surfaces or trivariate solids. As illustrated in Figure 1, the elements in the isogeometric homogenization are generated by combining the basis functions R_A and control points $\mathbf{P}_A$ (red dots in Figure 1). The physical domain's element, which is an image of the normalized square reference element in the parent space, undergoes an additional mapping in the parametric space due to the use of NURBS basis functions for discretization, a feature that is absent in conventional FE formulations.

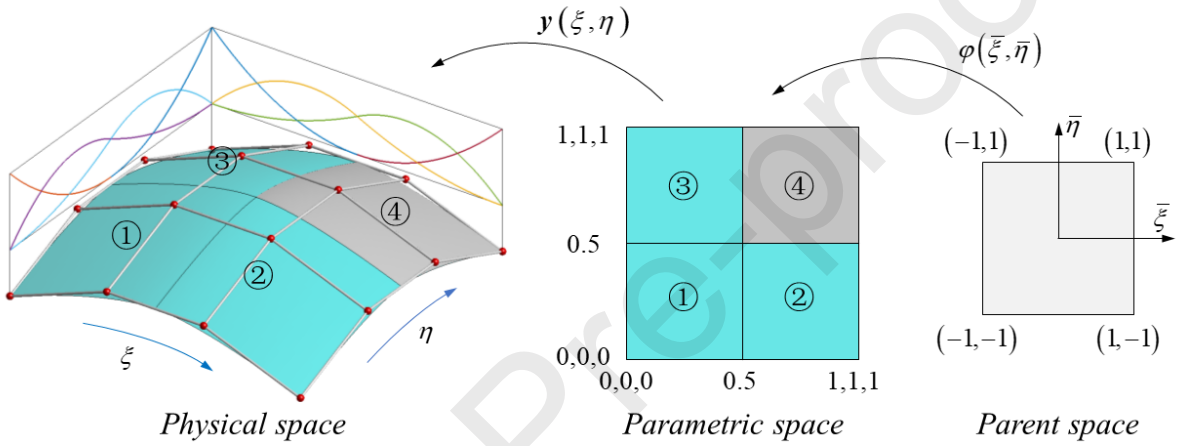

Figure 1 Diagrammatic interpretation of mesh discretization for a bi-quadratic NURBS surface (2x2 elements) and mappings from parent space through parametric space to physical space. The control points are denoted by the red points

Within the context of zeroth-order homogenization [30-32], the Laplace-transform of the displacement variables in the qth element can be expressed as a two-scale expansion, which contains the contributions from both macroscopic strain loading $\hat{\bar{\varepsilon}}_{ij}(s)$ and microstructure-induced fluctuating contribution $\hat{u}_i'^{(q)}(\mathbf{y},s)$ as follows:

$$\hat{u}_i^{(q)}(\mathbf{x},\mathbf{y},s)=\hat{\bar{\varepsilon}}_{ij}(s)x_j+\hat{u}_i'^{(q)}(\mathbf{y},s),\quad i=1,2,3 \tag{7}$$

The global coordinates $\mathbf{x}=(x_1,x_2,x_3)$ represent the overall response of the equivalent homogenous medium, while the local coordinates $\mathbf{y}=(y_1,y_2,y_3)$ describe the interior response of the unit cell. Different from that unknown variables are defined on the interpolated node in the conventional FE method, they are defined directly on the control points, called control variables in isogeometric analyses. Let $\hat{\mathbf{u}}_A'^{(q)}=\left[\hat{u}_{1,A}'^{(q)},\hat{u}_{2,A}'^{(q)},\hat{u}_{3,A}'^{(q)}\right]^{\mathrm{T}}$ be the Laplace-transform of fluctuating nodal displacement vectors at the Ath control point, then the fluctuating displacement variables of the NURBS-based geometry are approximated as:

$$\hat{\mathbf{u}}'^{(q)}(\mathbf{y},s)=\sum_{A}^{A=n}R_A\hat{\mathbf{u}}_A'^{(q)}(s) \tag{8}$$

where $\hat{\mathbf{u}}'^{(q)}=\left[\hat{u}_1',\hat{u}_2',\hat{u}_3'\right]^{\mathrm{T}(q)}$, n is the number of control points.

The above displacement field yields local strain in the qth element as shown below:

$$\hat{\varepsilon}_{ij}^{(q)}(\mathbf{y},s)=\hat{\bar{\varepsilon}}_{ij}(s)+\hat{\varepsilon}_{ij}'^{(q)}(\mathbf{y},s)=\hat{\bar{\varepsilon}}_{ij}(s)+\frac{1}{2}\left[\hat{u}_{i,j}'(\mathbf{y},s)+\hat{u}_{j,i}'(\mathbf{y},s)\right] \tag{9}$$

where $\hat{\varepsilon}_{ij}'^{(q)}(\mathbf{y},s)$ represents the Laplace transform of fluctuating strains that can be expressed as:

$$\hat{\boldsymbol{\varepsilon}}'^{(q)}(\mathbf{y},s)=\mathbf{B}^{(q)}\hat{\mathbf{U}}'^{(q)}(s) \tag{10}$$

where $\hat{\boldsymbol{\varepsilon}}'^{(q)}=\left[\hat{\varepsilon}_{11}',\hat{\varepsilon}_{22}',\hat{\varepsilon}_{33}',2\hat{\varepsilon}_{23}',2\hat{\varepsilon}_{13}',2\hat{\varepsilon}_{12}'\right]^{\mathrm{T}(q)}$, $\hat{\mathbf{U}}'^{(q)}=\left[\hat{\mathbf{u}}_1',\cdots,\hat{\mathbf{u}}_A',\cdots,\hat{\mathbf{u}}_n'\right]$, $\mathbf{B}^{(q)}$ denotes the displacement-strain matrix:

$$\mathbf{B}^{(q)}=\left\{\mathbf{B}_1^{(q)},\mathbf{B}_2^{(q)},\cdots,\mathbf{B}_A^{(q)},\cdots,\mathbf{B}_n^{(q)}\right\},\quad \mathbf{B}_A^{(q)}=\begin{bmatrix}R_{A,y_1} & 0 & 0 & 0 & R_{A,y_3} & R_{A,y_2}\\ 0 & R_{A,y_2} & 0 & R_{A,y_3} & 0 & R_{A,y_1}\\ 0 & 0 & R_{A,y_3} & R_{A,y_2} & R_{A,y_1} & 0\end{bmatrix}^{\mathrm{T}} \tag{11}$$

The total potential energy integral $\pi(s)$ in the transformed domain is computed through the assembly of the potential energy integral at the element level. This is achieved by enforcing control point equilibrium and fluctuating displacement continuity, together with periodic boundary conditions (s is omitted for simplicity) [33]:

$$\pi=\frac{1}{2}\int_V\hat{\bar{\boldsymbol{\varepsilon}}}^{\mathrm{T}}s\hat{\mathbf{C}}\hat{\bar{\boldsymbol{\varepsilon}}}\mathrm{d}V+\frac{1}{2}\hat{\mathbf{U}}'^{\mathrm{T}}\left(\int_V\mathbf{B}^{\mathrm{T}}s\hat{\mathbf{C}}\mathbf{B}\mathrm{d}V\right)\hat{\mathbf{U}}'+\hat{\mathbf{U}}'^{\mathrm{T}}\left(\int_V\mathbf{B}^{\mathrm{T}}s\hat{\mathbf{C}}\mathrm{d}V\right)\hat{\bar{\boldsymbol{\varepsilon}}}-\hat{\bar{\boldsymbol{\sigma}}}^{\mathrm{T}}\hat{\bar{\boldsymbol{\varepsilon}}}V \tag{12}$$

where V denotes the unit cell volume, $\hat{\mathbf{U}}'$ contains Laplace-transform of fluctuating displacements from all the control points and $\hat{\bar{\boldsymbol{\sigma}}}$ denotes the homogenized stresses in the transformed domain. Then, the total potential energy is minimized vis-à-vis the global fluctuating displacement vectors $\hat{\mathbf{U}}'(s)$, $\partial\pi/\partial\hat{\mathbf{U}}'(s)=0$, which yields the following global system of equations for the determination of unknown fluctuating displacements:

$$\hat{\mathbf{K}}\hat{\mathbf{U}}'(s)=\hat{\mathbf{f}} \tag{13}$$

where $\hat{\mathbf{K}}=\int_V\mathbf{B}^{\mathrm{T}}s\hat{\mathbf{C}}\mathbf{B}\mathrm{d}V$, $\hat{\mathbf{f}}=-\int_V\mathbf{B}^{\mathrm{T}}s\hat{\mathbf{C}}\mathrm{d}V\hat{\bar{\boldsymbol{\varepsilon}}}$.

To derive the homogenized or effective Hooke's relation in the Laplace-Carson domain, a prescribed unit macroscopic strain $\bar{\boldsymbol{\varepsilon}}(t)=H(t)\bar{\varepsilon}^0$ is imposed sequentially six times, whose Laplace transform is $\hat{\bar{\boldsymbol{\varepsilon}}}(s)=\bar{\varepsilon}^0/s$. The effective Hooke's law is obtained by averaging local constitutive relations in each element, which are determined through the solution of the unit cell problem in the Laplace-Carson space:

$$\hat{\bar{\boldsymbol{\sigma}}}(s)=\frac{1}{V}\sum_q\int s\hat{\mathbf{C}}^{(q)}\hat{\boldsymbol{\varepsilon}}^{(q)}\mathrm{d}V_q=s\hat{\mathbf{C}}^*\hat{\bar{\boldsymbol{\varepsilon}}} \tag{14}$$

2.4 Inversion scheme

Having acquired the homogenized (effective) stiffness and compliance tensors in the Laplace domain, the overall relaxation moduli and creep compliances in the time domain are obtained by leveraging the inversion scheme proposed by Zakian [28]. Specifically, to obtain the homogenized relaxation moduli in the specific time t, the unit cell problem in the Laplace-Carson domain is solved through the allocation $s(i)=\alpha_i/t$ for $i=1,\cdots,5$. The overall relaxation functions at a specific time t are evaluated using the following equations:

$$\mathbf{C}^*(t)=\frac{2}{t}\sum_{i=1}^{5}\mathrm{Re}\left[K_i\hat{\mathbf{C}}^*\left(\alpha_i/t\right)\right] \tag{15}$$

where the complex coefficients K_i and α_i are given in Table 1. The efficiency and accuracy of Zakian's inversion scheme have been demonstrated by Wang and Pindera [34] and Chen et al. [15] in the framework of LEHT and finite-volume homogenization theories, respectively.

Table 1 Coefficients for Zakian's inversion scheme [28]

	Complex coefficients		Complex coefficients
K_1	−36902. 08210+196990.4257i	α_1	12.83767675+1.666063445i
K_2	+61277. 02524+95408. 62551i	α_2	12.22613209+ 5.012718792i
K_3	−28916.56288+18169.18531i	α_3	10.93430308+8.409673116i
K_4	+4655.361138−1.901528642i	α_4	8.776434715+11.92185389i
K_5	118.7414011−141.3036911i	α_5	5. 225453361 +15.72952905i

3. Convergence study

The isogeometric homogenization theory utilizes the weak form solution of the unit cell boundary value problem, which provides approximate satisfaction of the equilibrium of the local problem upon sufficient mesh refinement. Additionally, the complexity of microstructures necessitates the use of multi-patches for discretizing the unit cell. While the proper order of NURBS basis functions can ensure the exact satisfaction of higher-order displacement derivatives and traction continuity conditions within a single patch, such conditions may not hold at the boundaries of adjacent patches. This is particularly true for the interface that divides the fiber and matrix.

In order to demonstrate the convergence behavior of the proposed technique, we employ below two measures that quantify the extent to which the local stress equilibrium and interfacial traction continuity conditions are satisfied, cf. Cavalcante et al. [33]. One way to measure the accuracy of the numerical simulation is through the average stress theorem, which states that the average stresses in the discretized element computed from surface or volume integration are equivalent when the pointwise equilibrium condition is satisfied. If pointwise equilibrium is not satisfied, an imbalance occurs and can be quantified by the difference given by the following integral:

$$\Delta\bar{\sigma}_{ij}^{(q)} = \frac{1}{V_q}\int_{S_q} t_i x_j \mathrm{d}S_q - \frac{1}{V_q}\int_{V_q} \sigma_{ij}\mathrm{d}V_q = \frac{1}{V_q}\int_{V_q} \frac{\partial \sigma_{ki}}{\partial x_k} x_j \mathrm{d}V_q \tag{16}$$

where S_q indicates the boundary of the qth element. The integral of the difference between the interfacial tractions at the heterogeneities and matrix interface provides the second measure:

$$\Delta\bar{t} = \frac{1}{S_0}\int_{S_0} \|\Delta\mathbf{t}\|\mathrm{d}S \tag{17}$$

where $\|\Delta\mathbf{t}\| = \sqrt{\Delta t_1^2 + \Delta t_2^2 + \Delta t_3^2}$ and S_0 represents the fiber-matrix interface.

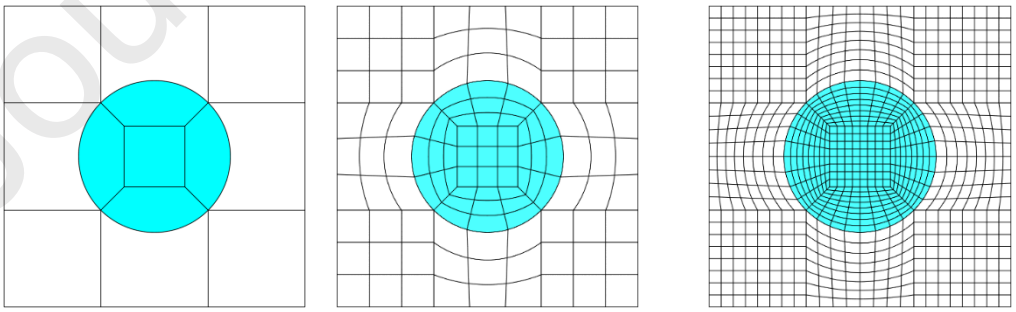

13 NURBS patches $nElems = 117$ $nElems = 832$

Figure 2 Mesh discretizations of unit cells in square arrangement containing 20% fiber volume fraction employed in the convergence study

In the first example, we consider glass/epoxy composite materials with 20% fiber volume fraction, and the unidirectional-oriented fibers are distributed in square manner. Young's moduli and Poisson's ratios for the fiber and matrix are: $E_f = 68.77$ GPa, $\nu_f = 0.21$ and $E_m = 3.27$ GPa, $\nu_m = 0.38$, respectively. The high-stress concentration and deformation gradients near the fiber/matrix interface, caused by the small diameter of the fibers relative to the entire unit cell dimension and significant property mismatch, make it a challenging test of the method's accuracy.

As shown in Figure 2, the square unit cell investigated herein is built with 13 NURBS patches, where the fiber contains 5 patches and the matrix contains 8 patches. Each patch is discretized into coarse (3×3) and fine (8×8) meshes. The boundaries of adjacent patches are kept consistent to avoid dealing with the coupling problems induced by mesh non-matching. Finally, the unit cell consists of 117 and 832 NURBS elements for the coarse and fine meshes, respectively. In order to thoroughly assess the predictive capability of the isogeometric homogenization theory, we apply unidirectional transverse normal strain loading by $\bar{\varepsilon}_{22} = 1\%$.

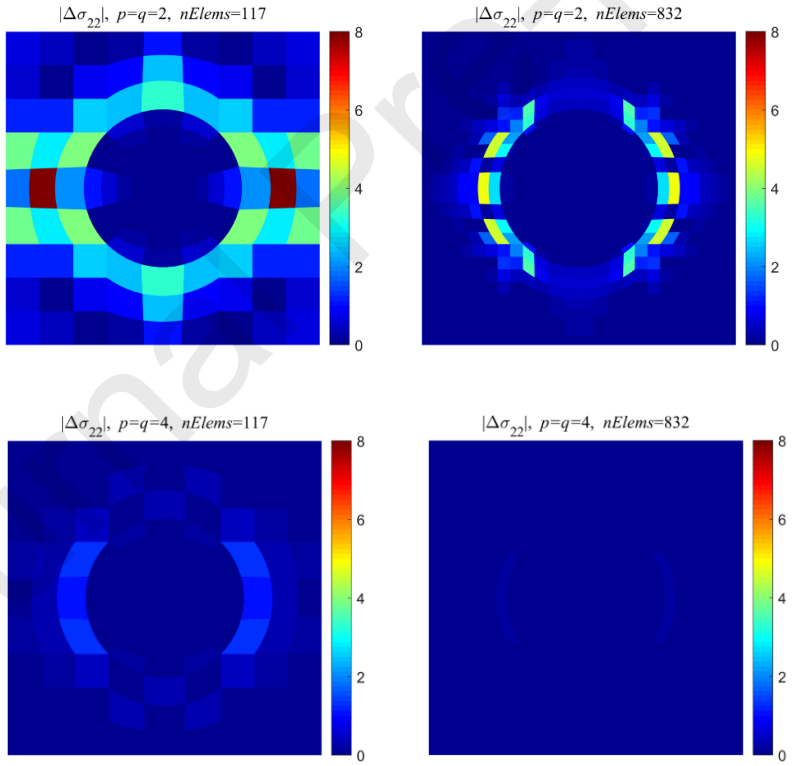

Figure 3 Comparison of unbalanced stress $|\Delta\sigma_{22}|$ distributions with two levels of mesh refinement and order of NURBS basis under the unidirectional macroscopic strain of $\bar{\varepsilon}_{22} = 1\%$

Figure 3 illustrates distributions of the unbalanced transverse normal stress $|\Delta\sigma_{22}|$ with two levels of mesh refinement and orders of NURBS basis function, namely, $p=q=2$ and $p=q=4$ respectively, thereby allowing straightforward evaluation of the effect of both mesh refinement and order of NURBS basis on the local stress equilibrium. As anticipated, the stress imbalance diminishes significantly by either increasing the mesh refinement from $nElems=117$ to $nElems=832$ and/or elevating the orders of the NURBS basis functions from $p=q=2$ to $p=q=4$. It is interesting to note that elevating the orders of the NURBS function tends to be more effective in decreasing the stress imbalance relative to increasing mesh refinement. In the case of $p=q=4$, the stress imbalance distributions almost vanished in the entire matrix and fiber domains, even with the coarse mesh $nElems=117$. Figure 4 shows variation of the interfacial traction differences with respect to mesh discretization at three different orders of NURBS basis, namely $p=q=2$, $p=q=3$ and $p=q=4$. Once again, the interfacial traction difference decreases rapidly with increasing mesh refinement or orders of NURBS basis. In the following simulations, considering the good performance of the fine mesh with $nElems=832$ and $p=q=4$, it will be utilized unless otherwise stated. The geometric modeling and simulation are implemented based on our previously developed framework NLIGA [35, 36].

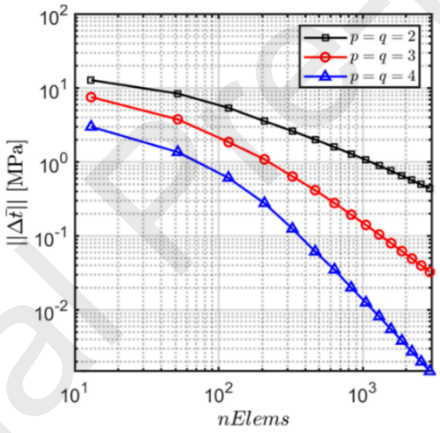

Figure 4 Variation of interfacial traction difference with respect to mesh discretization for different orders of NURBS basis under the unidirectional macroscopic strain of $\bar{\varepsilon}_{22}=1\%$

4. Numerical results

We proceed to assess the isogeometric homogenization theory's accuracy against benchmark solutions in the literature and conventional finite-element predictions. In the following simulations, unless otherwise stated, the fibers/inclusions exhibit elastic behavior, and the surrounding matrix resin was described by four-parameter, Prony series, and/or power law models in order to extensively assess the modelling capability of the IGH approach. The rheological representations for the first two models are illustrated in Figure 5. The four-parameter model to characterize the creep compliance of the matrix consists of series-connected Maxwell and Kelvin branches.

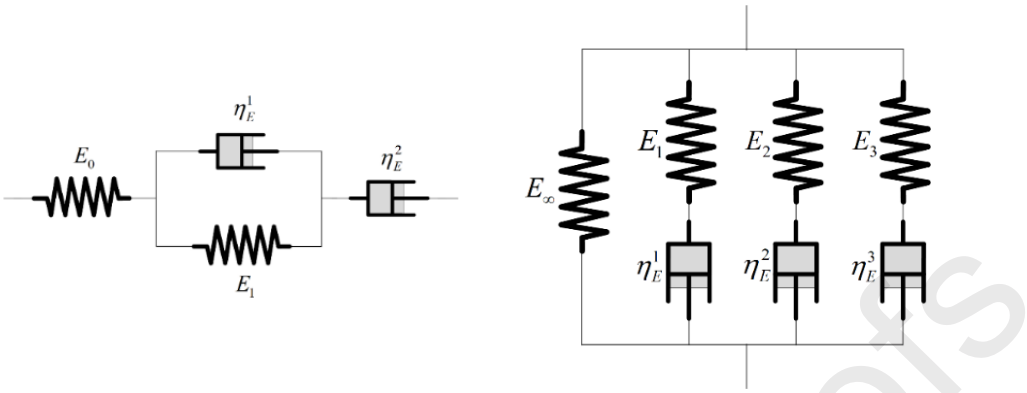

(a) (b)

Figure 5 Mechanical representation of (a) the four-parameter model; (b) the Prony series

$$S(t)=\frac{1}{E_0}+\frac{1}{E_1}\left(1-e^{-\frac{E_1}{\eta_E^1}t}\right)+\frac{t}{\eta_E^2} \tag{18}$$

where E_0, E_1, η_E^1 and η_E^2 are material parameters that can be characterized from stress-strain curves of pure matrix materials. The Prony series considered herein is well mimicked by the parallel connection of a spring and three Maxwell models. The Young's modulus relaxation function $E(t)$ is expressed in the following form:

$$E(t)=E_\infty+\sum_{i=1}^{3}E_i e^{-\frac{E_i}{\eta_E^i}t} \tag{19}$$

where E_∞, E_i and η_E^i are material parameters and $E_0=E_\infty+\sum_{i=1}^{3}E_i$ denotes the instantaneous elastic modulus. On the other hand, the power-law model characterizes the epoxy matrix creep compliance as:

$$S(t)=\frac{1}{E}+Ct^n \tag{20}$$

where E, C, and n are material constants. It is worth noting that the power law type creep compliance yields a non-separable hereditary function kernel, which poses challenges for incrementally solving the unit cell boundary value problem directly in the time domain. Hence, it is an ideal candidate for showcasing the benefits of the proposed approach, which is not dependent on the specific type of viscoelastic hereditary function kernel representing the viscoelastic response.

4.1 Analytical verification

The LEHT theory developed by Pindera and his collaborator [11] is an elasticity-based periodic homogenization technique for unidirectional composites, which was recently extended by Wang and Pindera [34] and He and Pindera [37] to account for hexagonal and square fiber arrangements with linearly-viscoelastic phases. The accuracy and reliability of the LEHT technique in predicting the homogenized moduli and local stress fields for periodic arrays have been verified extensively against the conventional finite-element and finite-volume direct averaging micromechanics approaches, among others. Herein, we will use LEHT results [34] as a benchmark to compare against the newly developed isogeometric homogenization technique.

We consider square unit cells with three volume fractions, namely $V_f = 20\%$, 40% and 60%. The fiber elastic moduli are $E_f = 68.77\text{GPa}$ and $v_f = 0.21$. The matrix was modelled as the four-parameter model with $E_0 = 3.27\text{GPa}$, $E_1 = 1.8\text{GPa}$, $\eta_E^1 = 300\text{GPa}\cdot\text{h}$ and $\eta_E^2 = 8000\text{GPa}\cdot\text{h}$. The Poisson's ratio of the epoxy was considered to be constant at $v_m = 0.38$. The relaxation functions for the glass/epoxy composites based on the above parameters are compared in Figure 6. It is observed that the isogeometric homogenization technique shows a high level of accordance with the LEHT predictions for a full set of relaxation moduli obtained in the interval [0 600] h in an increment of 25h. We note that to generate a complete set of relaxation moduli in an uncompiled MATLAB environment for six loading cases at a specific time, the LEHT theory takes an average of 32 seconds (based on three runs) due to its semi-analytical nature. Conversely, the IGH numerical approach requires 158 seconds for the same computations.

Comparison of the local stress field components σ_{22}, σ_{33} and σ_{23} under pure creep loading $\bar{\varepsilon}_{22} = H(t)\varepsilon_{22}^o \left(\varepsilon_{22}^o = 1\%\right)$ at $t = 600$ h generated by the two approaches for composites with 20% fiber volume fraction is presented in Figure 7. It is concluded that the results generated by the IGH and LEHT are indistinguishable. The smoothness of the stress fields predicted by the IGH across elements with different phase properties is comparable to the exact elasticity solution. It should be emphasized that in order to correctly evaluate the extent of continuity of field variables, the IGH and LEHT techniques compute and display the local stress field prediction without any interpolation across elements.

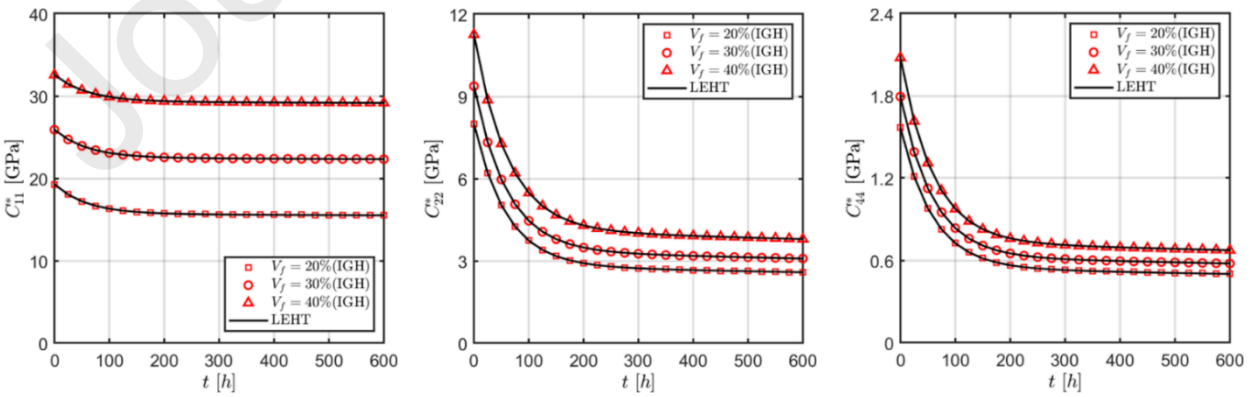

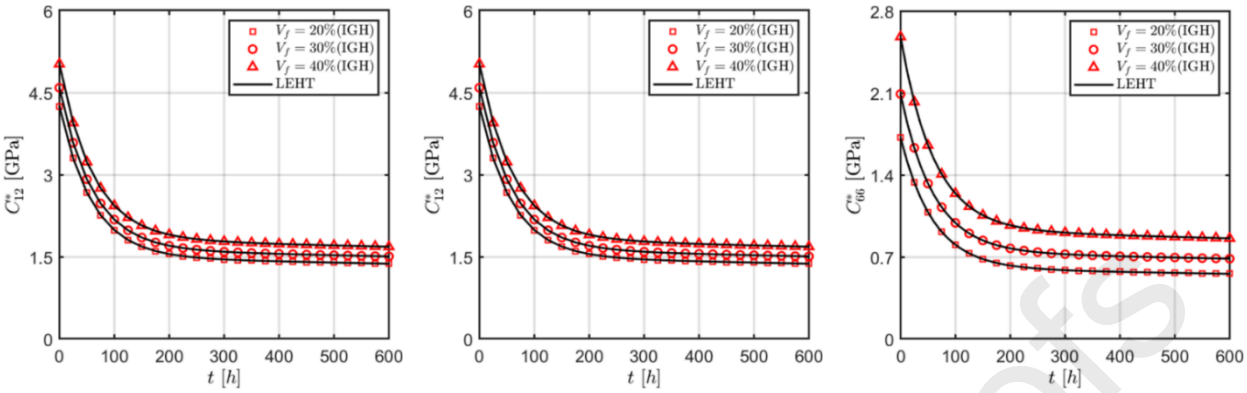

Figure 6 Comparison of variation of relaxation moduli with respect to time of unidirectional glass/epoxy composites with three volume fractions obtained from the IGH and LEHT predictions [34]

σ_{22} σ_{33} σ_{23}

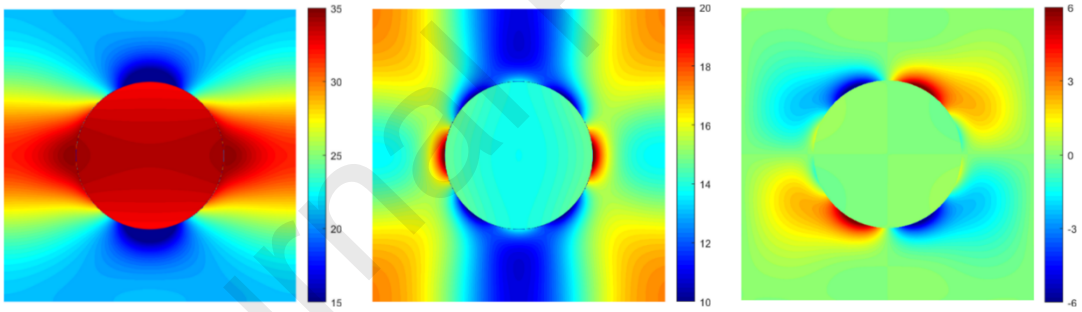

(a) LEHT

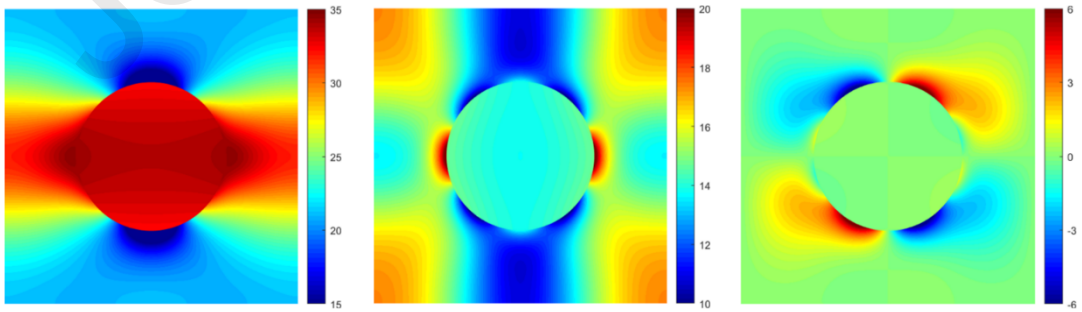

(b) IGH

Figure 7 Comparison of local stress components σ_{22}, σ_{33} and σ_{23} (MPa) of glass/epoxy composites under pure creep loading $\bar{\varepsilon}_{22} = H(t)\varepsilon_{22}^{o}\left(\varepsilon_{22}^{o} = 1\%\right)$ at $t = 600\text{h}$ obtained from the IGH and LEHT predictions [34]

4.2 Numerical verification

In this section, we further validate the accuracy of the proposed isogeometric micromechanics and homogenization theory against the conventional finite-element homogenization approach. As shown in Figure 8, we first consider unidirectional composites containing 40% of fiber volume fraction, with unidirectional fiber placed in square and hexagonal manners, respectively. For the square array, the IGH mesh has kept the same as before. For the hexagonal array, the IGH mesh was discretized into $nElems = 960$ using 15 patches where 9 patches are used for the inner fiber and 6 patches for the outer matrix. Each patch contains 8×8 bi-quartic NURBS elements. As before, the fiber deforms elastically with elastic moduli of $E_f = 100$ GPa and $v_f = 0.3$. The matrix was modelled as Prony series as shown in Figure 2b with three Maxwell branches and an elastic branch. The viscoelastic material parameters for the matrix are: $E_\infty = 2.16$ GPa , $E_1 = 0.2885$ GPa , $E_2 = 0.4327$ GPa , $E_3 = 0.7212$ GPa , $\eta_E^1 = 147$ GPa·min , $\eta_E^2 = 1026.4$ GPa·min , $\eta_E^3 = 7130.5$ GPa·min . The matrix Poisson's ratio was fixed at $v_m = 0.4$. While the elastic-viscoelastic correspondence principle has been employed in our IGH approach, the conventional finite-element results have been generated directly in the time space by solving the unit cell problem incrementally using the radial return mapping algorithm and the convex cutting plane technique, cf., Anagnostou et al. [38], thanks to the separable kernel of the Prony series. As the solution techniques for computing the homogenized viscoelastic response between the two approaches are fundamentally different, the IGH theory's validation is rigorous, which lends credence to the resulting conclusion.

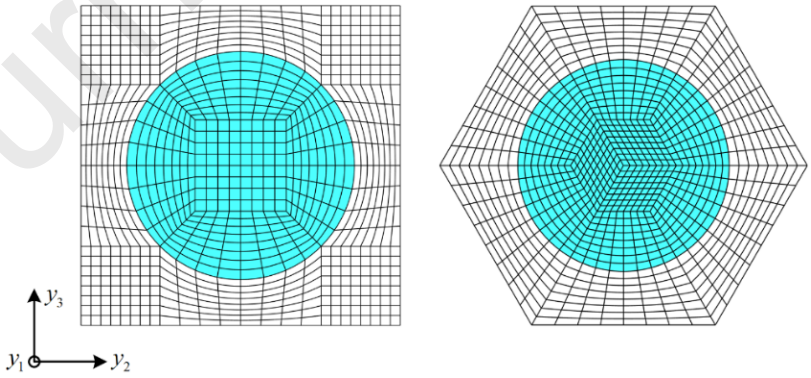

Figure 8 Mesh discretizations of square and hexagonal unit cells with 40% volume fraction employed in the calculations of homogenization creep compliance

Figure 9 illustrates the comparison of six creep compliance functions for hexagonal and square periodic microstructures generated at 20 times in the interval [0, 20000] min. The

correlation between the conventional FE with the incremental solution and isogeometric homogenization technique with correspondence principle, both employing the same level of mesh discretization, demonstrates excellent agreement. The effect of the fiber arrangement on effective in-plane creep compliance is significant. Increasing creep time tends to accentuate the effect of the fiber arrangement. We note that conventional finite-element techniques require the use of 100 time steps to obtain a converged response using the radial return mapping method. To provide a comprehensive evaluation of the computation cost, we compared the classical finite-element method with the incremental solution to the IGH method with the correspondence principle for the square array and hexagonal array cases. Notably, the classical finite-element method requires an average of 328 seconds and 412 seconds, respectively, to obtain the creep compliance matrix at the ultimate time step for the two arrays. In contrast, the IGH method completes the same computations in significantly less time, with only 157 seconds and 232 seconds, respectively, for the square and hexagonal arrays.

We also compared the transverse shear stress σ_{23} distributions generated by the conventional finite-element incremental solution under transverse shear loading $2\bar{\varepsilon}_{23} = 2H(t)\varepsilon^o_{23}\left(2\varepsilon^o_{23} = 1\%\right)$ at $t = 20000\,\text{min s}$ with the isogeometric homogenization results both for square and hexagonal arrays, as illustrated in Figure 10. As observed, nearly identical stress distributions between the two approaches are observed in both cases, providing additional evidence for the newly-developed isogeometric homogenization theory.

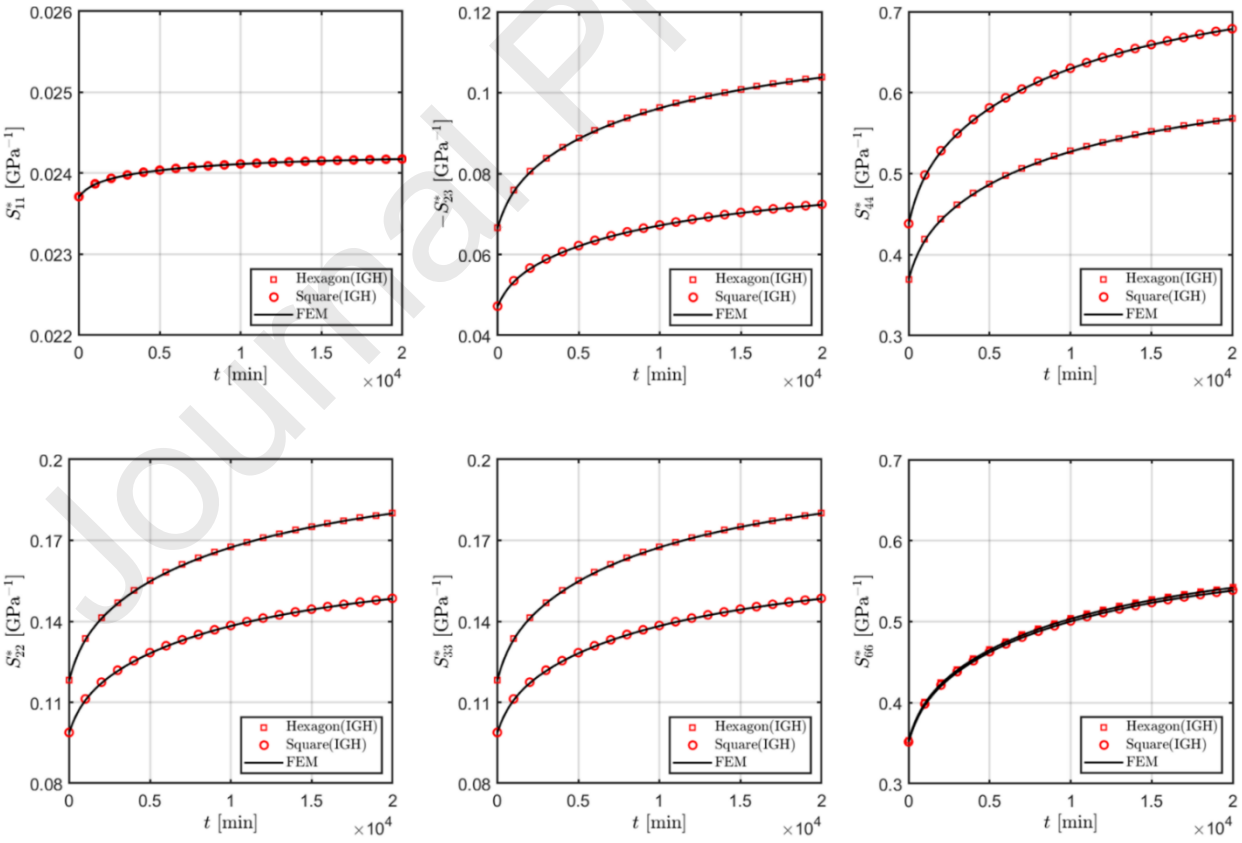

Figure 9 Comparison of creep compliance of unidirectional glass/epoxy composites with hexagonal and square arrays of fibers at constant fiber volume fractions (40%), predicted by the IGH and classical finite-element techniques. It is noted that the FEM results are obtained by incrementally solving the viscoelastic unit cell solution.

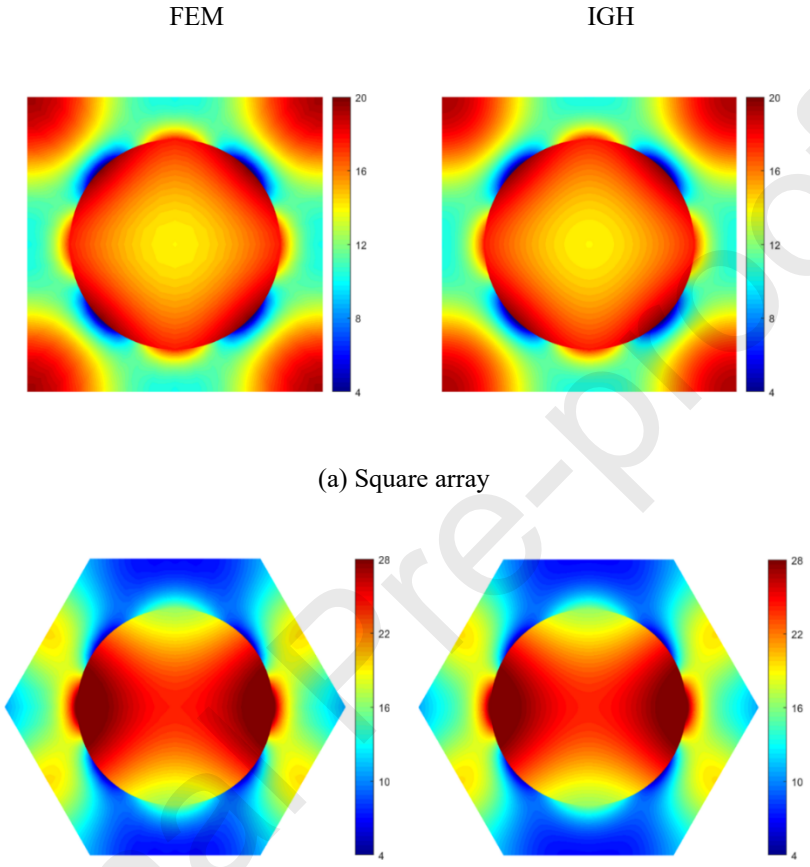

(a) Square array

(b) Hexagonal array

Figure 10 Comparison of transverse shear stress σ_{23} (MPa) in glass/epoxy composites with hexagonal and square arrays of fibers under pure creep loading $2\bar{\varepsilon}_{23} = 2H(t)\varepsilon^{o}_{23}\left(2\varepsilon^{o}_{23} = 1\%\right)$ at $t = 20000$ mins predicted by the IGH and the classical finite-element techniques

We end this section by considering a cubic unit cell reinforced by spherical inclusion of 30% particle volume fraction. As shown in Figure 11(a), the cubic unit cell is constructed with 7 trivariate NURBS patches, of which 6 for the matrix and 1 for the fiber. Each patch contains 4×4×4 tri-quartic NURBS elements. Note that with the advantage of NURBS in surface representation, the spherical interfaces between the fiber and matrix are geometrically exact. Finally, the whole unit cell is discretized into 448 tri-quartic NURBS elements for IGH. In contrast, the conventional

finite-element unit cell was discretized into $nElems = 2096$ linear brick (C3D8) and quadratic brick (C3D20) elements to capture the spherical inclusion geometry as well as to provide high-fidelity stress field variables (Figure 11b). To highlight the advantage of the isogeometric homogenization theory's independence of the type of hereditary function kernels representing the viscoelastic materials, we utilized the power law-type creep compliance of the epoxy, Eq. (20). This model is not easily adaptable to an incremental solution of the unit cell problem in the time space. Hence the conventional finite-element technique with viscoelastic phases was programmed using the elastic-viscoelastic correspondence principle as in the present approach. The Young's modulus and Poisson's ratio of the sphere are: $E_p = 68.77$ GPa, $v_p = 0.21$. The viscoelastic parameters of the surrounding matrix phase are: $E_0 = 3.36$ GPa, $C = 0.025$ GPa$\cdot$min, $n = 0.2$. As before, the Poisson's ratio of epoxy is kept constant at $v_m = 0.317$.

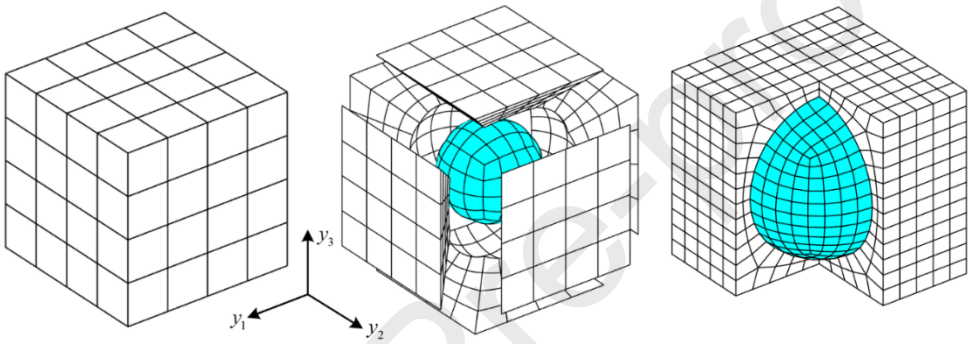

(a) IGH mesh (b) Conventional FE mesh

Figure 11 Unit cell mesh discretization with spherical inclusion of 30% volume fraction employed in the IGH and conventional finite-element simulation

Figure 12 presents comparison of variation of relaxation moduli with respect to time in the interval [0, 200] mins, generated by the conventional C3D8 and C3D20 finite element and the isogeometric homogenization techniques. It is observed that the homogenized relaxation moduli generated with the C3D20 finite element technique and the isogeometric homogenization method are nearly identical. A close look at the C3D8 element predictions reveals that the correlation between the C3D8 and the former approaches is less favorable. Figure 13 illustrates the normal stress profile σ_{11} under pure creep loading $\bar{\varepsilon}_{11} = H(t)\varepsilon_{11}^o \left(\varepsilon_{11}^o = 1\%\right)$, generated by the three techniques. We notice that the C3D8 linear brick element behaves badly in terms of local stress field recovery, namely the stress field variable exhibits a lack of continuity between adjacent elements due to the lack of C^1 continuity between the adjacent nodal displacements and the low order nature of the displacement interpolation function. The C3D20 element predicts significantly smoother stress field variable distribution than that of the C3D8. Nevertheless, the C3D20 elements exhibit the same disadvantages as the C3D8 element (the lack of C^1 continuity), albeit to a much lesser extent. This contrasts with the isogeometric homogenization technique. The predicted stress fields between the adjacent control elements within the same patches are

continuous to the machine accuracy, providing an additional justification for the development of the present approach.

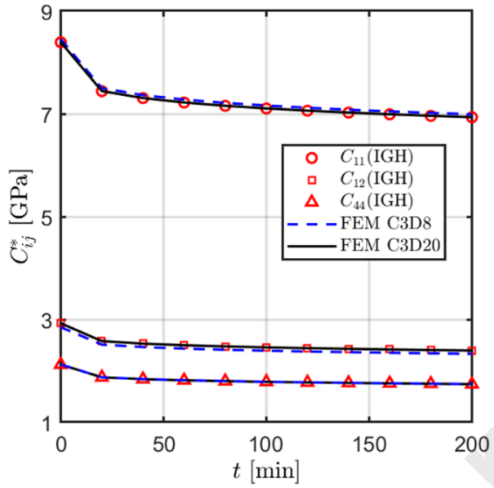

Figure 12 Comparison of relaxation moduli of three-dimensional polymer composites obtained from IGH theory using 448 tri-quartic NURBS elements with the conventional FE techniques using C3D8 and C3D20 elements

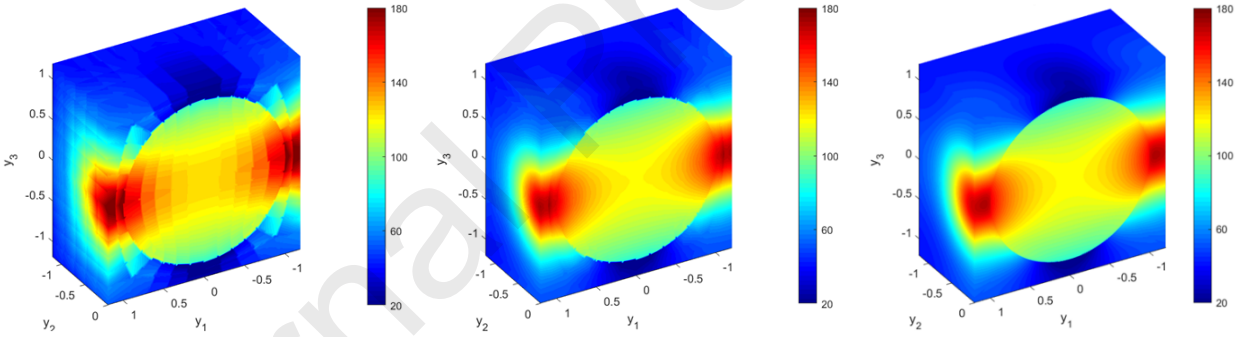

FEM C3D8 FEM C3D20 IGH

Figure 13 Comparison of stress σ_{11} (MPa) in discontinuous polymer composites under pure creep loading $\bar{\varepsilon}_{11} = H(t)\varepsilon^o_{11}\left(\varepsilon^o_{11} = 1\%\right)$ at $t = 200$ mins predicted by the IGH and the conventional finite-element technique

5. Conclusions

The correspondence principle was leveraged to propose the zeroth-order isogeometric homogenization theory with linearly viscoelastic phases. This theory facilitates efficient and accurate modelling of the relaxation and creep behavior of polymer composites with various microstructural parameters. The efficacy of implementing the correspondence principle in the IGH theory is contingent upon the efficient and accurate inversion of the Laplace-Carson space unit

cell solution back into the time space. The inversion technique developed by Zakian employed in this work was demonstrated to be an excellent vehicle to obtain the homogenized creep and relaxation response in the time domain. To illustrate the modelling and predictive capabilities of the proposed theory, while the fiber was kept elastic, the polymer matrix was represented as the four-parameter model, the Prony series, and the power law model, respectively. The comparison with the analytical and finite-element predictions demonstrates the accuracy and efficiency of the IGH technique.

There are several advantages of the IGH theory over conventional numerical homogenization techniques. First of all, the IGH utilizes the exact geometric representation of the unit cell microstructures with the NURBS patches, regardless of mesh discretization sizes, eliminating the extensive mesh refinement of the inclusion with curved surfaces. Secondly, the high orders and high continuities of spline basis functions provide a substantially more accurate local stress field, even in the presence of significant phase property contrast and distorted elements. The marriage of the IGH and correspondence principle enables solving separable and non-separable viscoelastic function kernels alike. The latter does not always seem possible to solve directly in the time domain.

Acknowledgment

Dr. Xiaoxiao Du would like to thank the financial support of the National Natural Science Foundation of China (Project No. 62102012) and the Young Elite Scientists Sponsorship Program by CAST (Project No. 2022QNRC001).

References

[1] Chen Q, Chatzigeorgiou G, Robert G, Meraghni F. Combination of mean-field micromechanics and cycle jump technique for cyclic response of PA66/GF composites with viscoelastic–viscoplastic and damage mechanisms. Acta Mechanica. 2023;234:1533-52.

[2] Chen Q, Chatzigeorgiou G, Robert G, Meraghni F. Viscoelastic-viscoplastic homogenization of short glass-fiber reinforced polyamide composites (PA66/GF) with progressive interphase and matrix damage: New developments and experimental validation. Mechanics of Materials. 2022;164:104081.

[3] Chen Q, Chatzigeorgiou G, Meraghni F. Extended mean-field homogenization of viscoelastic-viscoplastic polymer composites undergoing hybrid progressive degradation induced by interface debonding and matrix ductile damage. International Journal of Solids and Structures. 2021;210-211:1-17.

[4] Dey AP, Welschinger F, Schneider M, Gajek S, Böhlke T. Rapid inverse calibration of a multiscale model for the viscoplastic and creep behavior of short fiber-reinforced thermoplastics based on Deep Material Networks. International Journal of Plasticity. 2023;160:103484.

[5] Pallicity TD, Böhlke T. Effective viscoelastic behavior of polymer composites with regular periodic microstructures. International Journal of Solids and Structures. 2021;216:167-81.

[6] Hill R. Theory of mechanical properties of fiber-strengthened materials: I. elastic behavior. J Mech Phys Solids. 1964;12:199-212.

[7] Christensen R, Lo K. Solutions for effective shear properties in three phase sphere and cylinder models. Journal of the Mechanics and Physics of Solids. 1979;27:315-30.

[8] Mori T, Tanaka K. Average stress in matrix and average elastic energy of materials with misfitting inclusions. Acta Metallurgica. 1973;21:571-4.

[9] Chen Q, Chatzigeorgiou G, Meraghni F. Hybrid hierarchical homogenization theory for unidirectional CNTs-coated fuzzy fiber composites undergoing inelastic deformations. Composites Science and Technology. 2021;215:109012.

[10] Chen Q, Wang G, Pindera M-J. Homogenization and localization of nanoporous composites - A critical review and new developments. Composites Part B: Engineering. 2018;155:329-68.

[11] Drago AS, Pindera M-J. A Locally Exact Homogenization Theory for Periodic Microstructures With Isotropic Phases. Journal of Applied Mechanics. 2008;75.

[12] Tikarrouchine E, Chatzigeorgiou G, Praud F, Piotrowski B, Chemisky Y, Meraghni F. Three-dimensional FE2 method for the simulation of non-linear, rate-dependent response of composite structures. Composite Structures. 2018;193:165-79.

[13] Otero JA, Rodríguez-Ramos R, Guinovart-Díaz R, Cruz-González OL, Sabina FJ, Berger H, et al. Asymptotic and numerical homogenization methods applied to fibrous viscoelastic composites using Prony's series. Acta Mechanica. 2020;231:2761-71.

[14] Cruz-González OL, Rodríguez-Ramos R, Otero JA, Ramírez-Torres A, Penta R, Lebon F. On the effective behavior of viscoelastic composites in three dimensions. International Journal of Engineering Science. 2020;157:103377.

[15] Chen Q, Wang G, Chen X, Geng J. Finite-volume homogenization of elastic/viscoelastic periodic materials. Composite Structures. 2017;182:457-70.

[16] Cavalcante MAA, Marques SPC. Homogenization of periodic materials with viscoelastic phases using the generalized FVDAM theory. Computational Materials Science. 2014;87:43-53.

[17] Hughes TJR, Cottrell JA, Bazilevs Y. Isogeometric analysis: CAD, finite elements, NURBS, exact geometry and mesh refinement. Computer Methods in Applied Mechanics and Engineering. 2005;194:4135-95.

[18] Cottrell JA, Hughes TJ, Bazilevs Y. Isogeometric analysis: toward integration of CAD and FEA: John Wiley & Sons, 2009.

[19] Piegl L, Tiller W. Rational B-spline Curves and Surfaces. In: Piegl L, Tiller W, editors. The NURBS Book. Berlin, Heidelberg: Springer Berlin Heidelberg; 1995. p. 117-39.

[20] Sederberg TW, Zheng J, Bakenov A, Nasri A. T-splines and T-NURCCs. ACM Trans Graph. 2003;22:477–84.

[21] Deng J, Chen F, Li X, Hu C, Tong W, Yang Z, et al. Polynomial splines over hierarchical T-meshes. Graphical Models. 2008;70:76-86.

[22] Lipton S, Evans JA, Bazilevs Y, Elguedj T, Hughes TJR. Robustness of isogeometric structural discretizations under severe mesh distortion. Computer Methods in Applied Mechanics and Engineering. 2010;199:357-73.

[23] Matsubara S, Nishi S-N, Terada K. On the treatments of heterogeneities and periodic boundary conditions for isogeometric homogenization analysis. International Journal for Numerical Methods in Engineering. 2017;109:1523-48.

[24] Alberdi R, Zhang G, Khandelwal K. A framework for implementation of RVE-based multiscale models in computational homogenization using isogeometric analysis. International Journal for Numerical Methods in Engineering. 2018;114:1018-51.

[25] Schmidt F, Krüger M, Keip M-A, Hesch C. Computational homogenization of higher-order continua. International Journal for Numerical Methods in Engineering. 2022;123:2499-529.

[26] Tsapetis D, Sotiropoulos G, Stavroulakis G, Papadopoulos V, Papadrakakis M. A stochastic multiscale formulation for isogeometric composite Kirchhoff–Love shells. Computer Methods in Applied Mechanics and Engineering. 2021;373:113541.

[27] Wang Z-P, Wang Y, Poh LH, Liu Z. Integrated shape and size optimization of curved tetra-chiral and anti-tetra-chiral auxetics using isogeometric analysis. Composite Structures. 2022;300:116094.

[28] Zakian V. Numerical inversion of Laplace transform. Electronics Letters. 1969;5:120-1.

[29] Christensen R. Theory of viscoelasticity: an introduction. New York, NY: Academic Press, 1971.

[30] Bensoussan A, Lions J-L, Papanicolaou G. Asymptotic analysis for periodic structures: North Holland, Amsterdam,Netherlands, 1978.

[31] He Z, Pindera M-J. Finite Volume-Based Asymptotic Homogenization of Periodic Materials Under In-Plane Loading. Journal of Applied Mechanics. 2020;87.

[32] Chen Q, Pindera M-J. Homogenization and localization of elastic-plastic nanoporous materials with Gurtin-Murdoch interfaces: An assessment of computational approaches. International Journal of Plasticity. 2020;124:42-70.

[33] Cavalcante MAA, Khatam H, Pindera M-J. Homogenization of elastic–plastic periodic materials by FVDAM and FEM approaches – An assessment. Composites Part B: Engineering. 2011;42:1713-30.

[34] Wang G, Pindera M-J. Locally-exact homogenization of viscoelastic unidirectional composites. Mechanics of Materials. 2016;103:95-109.

[35] Du X, Zhao G, Zhang R, Wang W, Yang J. Numerical implementation for isogeometric analysis of thin-walled structures based on a Bézier extraction framework: nligaStruct. Thin-Walled Structures. 2022;180:109844.

[36] Du X, Zhao G, Wang W, Guo M, Zhang R, Yang J. NLIGA: A MATLAB framework for nonlinear isogeometric analysis. Computer Aided Geometric Design. 2020;80:101869.

[37] He Z, Pindera M-J. Locally exact asymptotic homogenization of viscoelastic composites under anti-plane shear loading. Mechanics of Materials. 2021;155:103752.

[38] Anagnostou D, Chatzigeorgiou G, Chemisky Y, Meraghni F. Hierarchical micromechanical modeling of the viscoelastic behavior coupled to damage in SMC and SMC-hybrid composites. Composites Part B: Engineering. 2018;151:8-24.

Qiang Chen: Methodology; Software; Formal analysis; Writing - Original Draft

Xiaoxiao Du: Software; Validation; Supervision; Funding acquisition; Writing - Original Draft;

Wei Wang: Conceptualization; Validation; Writing - Review & Editing

George Chatzigeorgiou: Methodology; Conceptualization; Writing - Review & Editing

Fodil Meraghni: Methodology; Conceptualization; Writing - Review & Editing

Gang Zhao: Conceptualization; Writing - Review & Editing

Declaration of interests

☒ The authors declare that they have no known competing financial interests or personal relationships that could have appeared to influence the work reported in this paper.

☐ The authors declare the following financial interests/personal relationships which may be considered as potential competing interests: